ELSEVIER

Chemical Geology 185 (2002) 205–225

CHEMICAL GEOLOGY
INCLUDING
ISOTOPE GEOSCIENCE

www.elsevier.com/locate/chemgeo

O and Pb isotopic analyses of uranium minerals by ion microprobe and U–Pb ages from the Cigar Lake deposit

Mostafa Fayek [a,*], T. Mark Harrison [a], Rodney C. Ewing [b,1], Marty Grove [a], Chris D. Coath [a]

[a] *Department of Earth and Space Science, University of California, Los Angeles, CA 90095-1567, USA*
[b] *Department of Nuclear Engineering and Radiological Sciences, The University of Michigan, 2958A Cooley Building, 2355 Bonisteel Boulevard, Ann Arbor, MI 48109-2104, USA*

Received 30 May 2001; accepted 22 October 2001

Abstract

We apply a rapid and accurate in situ technique to make U–Pb isotopic measurements of complexly intergrown uranium minerals and oxygen isotopic analyes of uraninite from the unconformity-type Cigar Lake uranium deposit. Secondary uranium minerals intergrown with uraninite, such as coffinite, $USiO_4 \cdot nH_2O$ and calciouranoite, $CaU_2O_7 \cdot 5H_2O$, were identified by high-resolution transmission electron microscopy (HRTEM). In situ U–Pb results from three stages of uraninite and coffinite define well-correlated arrays on concordia with upper intercepts of 1461 ± 47, 1176 ± 9, and 876 ± 14 Ma ($\pm 1\sigma$). These ages are interpreted as the minimum ages of mineralization correlate with the timing of clay mineral alteration ($\sim$ 1477 Ma) associated with these unconformity-type uranium deposits, the ages of magnetization events at 1600–1450 and 900 Ma from the Athabasca Basin, and the Grenvillian Orogeny at $\sim$ 1100 Ma. In situ U–Pb isotopic analyses of uraninite and coffinite can document the Pb*/U heterogeneities that occur on the scale of 15–30 μm, thus providing relatively accurate information regarding the timing of fluid interactions associated with the evolution of these deposits. The high spatial resolution and precision of the ion microprobe allow us to measure $\delta^{18}O$ values of 20–100 μm unaltered portions of uraninites from Cigar Lake. The range of $\delta^{18}O$ values (-33.9 to -20.4‰) are among the lowest reported for unconformity-type deposits, confirming that conventional fluorination analyses of material sampled at the mm-scale are insufficient to avoid contamination from isotopically heavier coffinite and calciouranoite.

Keywords: Uraninite; SIMS; U–Pb; Oxygen; Isotopes; Cigar Lake

1. Introduction

Uranium deposits have been used as "natural analogues" in order to understand the mechanism and extent of migration of uranium and other radionuclides from a spent fuel repository because uraninite, UO_{2+x} (the most common U^{4+}-bearing mineral, found in most uranium deposits) and UO_2 (the major constituent

* Corresponding author. Current address: 306 Geology Bldg., Department of Geological Sciences, University of Tennessee, Knoxville, TN 37996, USA. Tel.: +1-865-576-4839; fax: +1-865-576-8559.
E-mail addresses: mfayek@utk.edu (M. Fayek), rodewing@umich.edu (R.C. Ewing).
[1] Tel.: +1-313-647-8529.

0009-2541/02/$ - see front matter
PII: S0009-2541(01)00401-6

of spent fuel) are chemically and structurally similar (Finch and Ewing, 1992; Janeczek et al., 1996). However, the extent and processes of alteration of uraninite in these deposits are, in general, poorly understood.

Uraninite varies widely in composition from $UO_{2.07}$ to $UO_{2.25}$ (Grandstaff, 1976; Dyck, 1978; Smith, 1984; Burns et al., 1996). Although the uraninite structure can accommodate some degree of oxidation, in highly oxidizing-aqueous environments, uraninite is unstable and susceptible to alteration and oxidation, commonly altering to hydrated uranyl phases. Corrosion experiments on synthetic UO_2 (Bruno et al., 1991; Wronkiewicz et al., 1992; Bruno et al., 1995), UO_2 fuel (Johnson et al., 1982; Johnson and Werme, 1994) and natural uraninite (Fayek et al., 1997a) have shown that uraninite and synthetic UO_2 in the presence of an oxidizing fluid readily alter to hydrated uranyl-oxides and hydrated uranyl-silicates which include curite, schoepite, becquerelite, and soddyite, which are similar to uranyl minerals associated with natural uraninite.

The Cigar Lake unconformity-type uranium deposit, located near the eastern rim of the Athabasca Basin in Saskatchewan (Fig. 1), has recently been the focus of an international program to study uranium deposits as natural analogues for subsurface spent nuclear fuel repositories (Cramer, 1995; Smellie and Karlsson, 1996). The Cigar Lake deposit was selected as a natural analogue because it is well preserved without evident, significant radionuclide migration to the surface during the past 10 000 years (Goodwin et al., 1988; Cramer, 1995). In addition, the uranium ore is surrounded by natural barriers, including a clay zone and several hundred meters of sandstone host rock, which are similar in many respects to the conceptual disposal proposed for the disposal of spent nuclear fuel in Canada (Cramer, 1995). Therefore, the Cigar Lake deposit is considered to be important because many of its features are analogous to the barrier systems which are proposed for nuclear waste repositories.

Although many aspects of this deposit have been documented in detail (e.g. Cramer, 1995; Smellie and Cramer, 1994), establishing the timing of initial uranium emplacement and subsequent alteration history have been challenging and incompletely realized goals. For example, it is very unusual to obtain concordant U–Pb data from uraninite and the degree

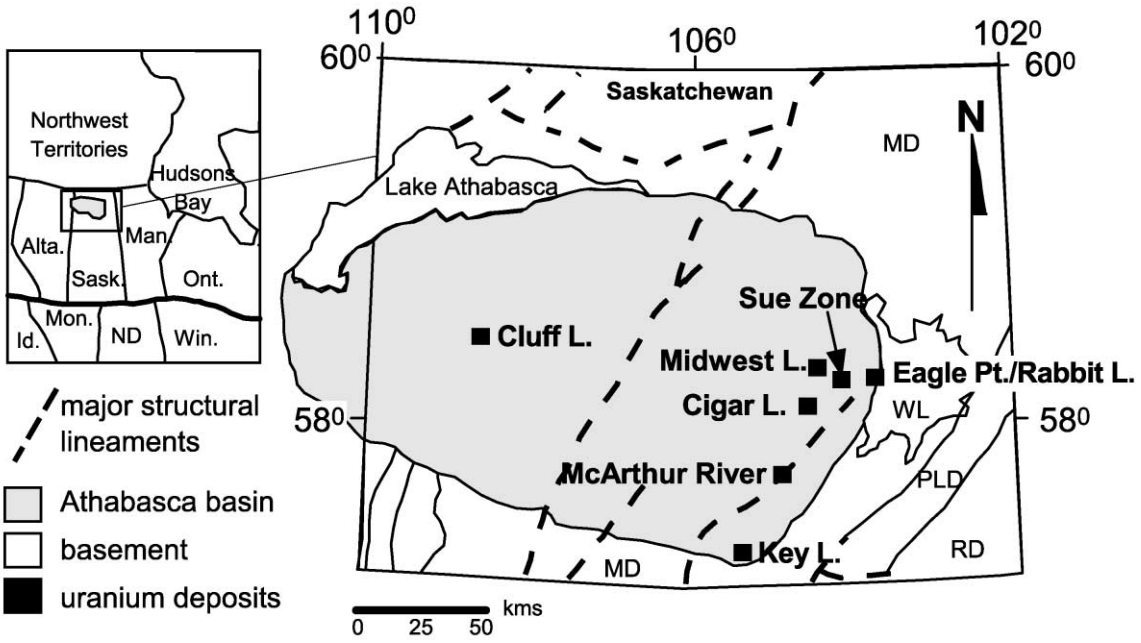

Fig. 1. Map showing the extent of the Athabasca Basin, location of the uranium deposits and major lithostructural domains in the crystalline basement of Saskatchewan (modified from Hoeve and Sibbald, 1978). Abbreviations: MD = Mudjatik Domain; WD = Wollaston Domain; PLD = Peter Lake Domain; RD = Rottenstone Domain; and WL = Wollaston Lake; R = River; L = Lake.

of discordance is often much greater than 5% leading to uncertainty in the interpretation of the U–Pb values (e.g., Cumming and Krstic, 1992).

The wide range of ages associated with multiple mineralizing episodes from the Cigar Lake deposit (Cummings and Krstic, 1992; Fayek et al., 1997a) underscores both the mobility of U and Pb* during subsequent alteration events and the limitations of the analytical methods. In addition, uraninites from the Cigar Lake deposit have a wide range of $\delta^{18}O$ values ($-28.5‰$ to $-3.8‰$; Fayek et al., 1997a). The light $\delta^{18}O$ values are likely the result of post depositional recrystallization of the uraninite by meteoric waters having $\delta^{18}O$ values $\sim -20‰$ (Kotzer and Kyser, 1993; Fayek and Kyser, 1997; Fayek et al., 1997a), where as the heavy $\delta^{18}O$ values may be due to the inclusion of fine intergrowths of coffinite and clay minerals that could not be separated during the microdrilling of the uraninite for oxygen isotopic analyses by the fluorination technique. Therefore, precise, high spatial resolution U–Pb and O isotopic measurements of minerals with complex chemistry such as uraninite would greatly aid in unraveling the complex fluid histories associated with certain uranium deposits.

The purpose of this study is to characterize the secondary, actinide-bearing phases that formed during the alteration of uraninite and utilize the ion microprobe to characterise the oxygen isotopic composition of uraninite and determine the age of uranium minerals from the Cigar Lake deposit. These techniques combine the advantages of conventional U–Pb dating (i.e., use of concordia) and in situ analysis, and therefore are suited for the study of chemically complex uranium-oxides associated with unconformity-type uranium deposits.

2. Background

2.1. In situ isotopic analyses by SIMS

Secondary ionization mass spectrometry (SIMS) or the ion microprobe is a technique that was developed to provide in situ measurement of isotopic ratios with a spatial resolution on the scale of a few micrometers. SIMS analyses uses a focused beam of primary ions (a few micrometers in diameter) to bombard a solid sample surface in order to obtain a localized analysis. The bombardment or "sputtering" removes atoms from the polished surface of the specimen. Some of these atoms are ionized during the process and can be focused and accelerated as a "secondary" beam through a slit and into a mass spectrometer (Reed, 1989). For stable isotopic (i.e. negative ion) measurements, the selected area is sputtered with a 10-keV Cs^+ primary beam which generates a secondary negative ion beam of the desired element (e.g. O, N, C, S) whereas for U and Pb measurements, a 10-keV O^- primary beam is used which generates a secondary positive ion beam of the desired element (e.g. U, Pb, Th, etc.).

During the measurement process, an intrinsic mass-dependent bias is introduced and is referred to as instrumental mass fractionation (IMF). A variety of processes combines to produce the observed IMF. These include secondary atom extraction (sputtering) and ionization (Sigmund, 1969; Shroeer et al., 1973; Williams, 1979; Yu and Lang, 1986), secondary ion transmission (Shimizu and Hart, 1982), and detection (Valley and Graham, 1991; Lyon et al., 1994). The greatest contributors to the IMF are sputtering and ionization which depend most strongly upon sample characteristics (i.e., chemical composition). This is referred to as compositionally dependent fractionations or "matrix effects" (e.g., Valley et al., 1997). Therefore, in ion microprobe analysis, IMF is corrected for by comparing measurements of a chemically and isotopically homogenous mineral standard that is compositionally similar to the unknown. Ion microprobe results from the standard are compared to its accepted isotopic composition in order to compute a correction factor that is applied to the unknowns measured during the same analysis session (e.g., Leshin et al., 1998).

3. Analytical techniques

3.1. Standard material selection and grain mount preparation

Candidate material, synthetic UO_2, to be used as a uraninite standard was crushed, sieved to the <350 mesh ($5–10$ μm) size fraction and sample purity was assessed by X-ray diffraction. For ion microprobe grain mounts, 500 μm to $\sim$ 1 mm-sized crystals of synthetic

Table 1
Ion and electron microprobe data from the Cigar Lake deposit

Sample	Spot No.	Mineral	$\delta^{18}O$ (‰)	$^{207}Pb/^{206}Pb$	Error % (1σ)	$^{208}Pb/^{206}Pb$	Error % (1σ)	$^{207}Pb/^{206}Pb$ Age (Ma)	Electron microprobe data[a]			
									UO_2	PbO	SiO_2	CaO
W 83C	1	uran	−23.1	0.08444	0.16	0.000239	3.4	1303 ± 3	80.2	12.8	0.21	1.04
	2	uran	−25.5	0.08436	0.15	0.000228	2.2	1301 ± 3	78.8	14.1	0.05	0.69
	3	uran	−23.9	0.08555	0.15	0.000167	3.6	1328 ± 3	79.4	14.9	0.02	0.75
	4	uran	−25.2	0.08514	0.16	0.000090	3.8	1319 ± 3	80.4	14.2	0.06	0.85
	5	uran	−25.5	0.08506	0.13	0.000076	3.7	1317 ± 3	81.0	14.1	0.06	0.75
	6	uran	−24.8	0.08568	0.15	0.000079	4.1	1331 ± 3	80.0	13.9	0.11	0.79
	7	uran	−25.6	0.08590	0.14	0.000064	3.7	1336 ± 3	79.8	14.1	0.01	0.76
	8	uran	−25.3	0.08552	0.13	0.000088	3.6	1327 ± 3	79.3	13.8	0.10	0.75
	9	uran	−24.7	0.08577	0.55	0.000305	1.7	1333 ± 10	80.6	14.9	0.06	0.77
	10	uran	−28.0	0.08534	0.13	0.000075	5.0	1323 ± 2	79.3	13.8	0.06	0.79
	11	uran	−27.3	0.08514	0.16	0.000087	4.8	1319 ± 3	80.5	14.3	0.04	0.72
	12	uran	−25.9	0.08543	0.14	0.000242	2.1	1325 ± 3	79.5	13.8	0.09	0.77
	13	uran	−22.9	0.08382	0.18	0.000142	3.5	1288 ± 4	80.4	13.4	0.10	0.84
	14	uran	−25.0	0.08389	0.15	0.000120	3.4	1290 ± 3	79.5	13.2	0.08	0.86
	15	uran	−23.4	0.08400	0.14	0.000092	4.4	1293 ± 3	79.7	12.8	0.13	0.91
CS615A1	1	uran	−33.9	0.08220	0.24	0.000249	3.6	1250 ± 9	78.3	12.4	0.22	1.09
	2	uran	−29.2	0.08169	0.26	0.000588	2.6	1238 ± 13	80.1	12.4	0.29	1.05
	3	uran	−30.5	0.08397	0.20	0.000196	5.6	1292 ± 8	77.3	14.1	0.04	0.85
	4	uran	−32.5	0.08245	0.22	0.000256	3.4	1256 ± 9	78.9	13.0	0.15	0.90
	5	uran	−27.9	0.08124	0.22	0.000148	4.7	1227 ± 8	81.8	11.8	0.07	0.89
	6	uran	−29.7	0.08246	0.26	0.000158	6.1	1256 ± 16	78.8	11.8	0.23	1.13
	7	uran	−33.7	0.08302	0.21	0.000100	5.2	1270 ± 8	78.7	14.0	0.03	1.08
	8	uran	−30.1	0.07929	0.24	0.000301	3.3	1179 ± 8	79.9	11.8	0.48	1.43
	9	coff	N.A	0.06585	0.59	0.004573	2.0	802	83.4	1.1	3.62	1.68
	10	Ca–U	N.A	0.05129	0.84	0.001485	15.3	254	82.1	1.3	3.34	2.34
CS615B	1	uran	−20.4	0.07845	0.28	0.000975	2.4	1158 ± 5	78.2	12.6	0.23	1.13
	2	uran	−23.0	0.07944	0.27	0.000197	5.1	1183 ± 5	80.0	12.0	0.19	1.24
	3	uran	−24.1	0.07807	0.26	0.000152	7.3	1149 ± 5	79.4	12.2	0.20	1.11
	4	uran	−26.7	0.07938	0.26	0.000177	5.4	1182 ± 5	79.0	12.8	0.17	0.99
	5	uran	−24.9	0.07942	0.26	0.000128	6.3	1183 ± 5	79.0	12.7	0.18	1.12
	6	uran	−26.4	0.07874	0.35	0.000186	5.9	1166 ± 7	79.9	11.8	0.23	1.14
	7	uran	−24.8	0.07964	0.33	0.000165	5.6	1188 ± 7	80.2	12.8	0.17	0.95
	8	uran	−25.7	0.07945	0.35	0.000310	4.4	1183 ± 7	80.3	11.6	0.29	1.32
CS449	1	uran	−23.8	0.08173	0.28	0.000401	3.8	1239 ± 5	81.2	11.7	0.24	1.22
	2	uran	−27.0	0.07976	0.25	0.000053	9.3	1191 ± 5	80.1	11.7	0.17	1.17
	3	uran	−23.1	0.08104	0.24	0.000056	8.7	1222 ± 5	80.1	12.6	0.18	1.26
	4	uran	−26.7	0.08105	0.27	0.000234	4.8	1223 ± 5	80.2	11.2	0.37	1.43
	5	uran	−28.9	0.07839	0.26	0.000048	10.0	1157 ± 5	78.8	13.1	0.16	1.19
	6	uran	−24.2	0.07771	0.25	0.000068	8.0	1140 ± 5	82.3	8.6	0.22	2.27
	7	uran	−23.8	0.08293	0.23	0.000090	6.7	1268 ± 4	79.4	11.7	0.27	1.13
	8	uran	−27.3	0.07932	0.26	0.000102	7.0	1180 ± 5	79.6	14.3	0.16	0.99
	9	coff	N.A	0.07692	0.58	0.003918	3.0	1119 ± 10	82.8	1.6	3.23	2.32
	10	coff	N.A	0.07649	0.65	0.004692	5.2	1108 ± 10	81.5	1.9	2.63	2.70
	11	coff	N.A	0.07550	0.46	0.003864	2.2	1082 ± 9	81.5	1.7	2.87	2.32
CS235m	1	uran	−20.6	0.06879	0.34	0.000637	3.2	893 ± 7	81.2	9.2	0.39	1.77
	2	uran	−23.2	0.06850	0.33	0.000477	3.9	884 ± 7	80.2	9.6	0.28	1.76
	3	uran	−23.8	0.06795	0.36	0.002083	2.0	867 ± 7	82.5	8.7	0.49	1.79

U (%)	Pb (%)	^{206}Pb	^{207}Pb	^{208}Pb	^{235}U	^{238}U	^{207}Pb/^{235}U	Error (%)	^{206}Pb/^{238}U	Error (%)	$\rho(x,y)$
70.7	11.9	11.0	0.93	0.00262	0.509	70.2	1.818	1.8	0.156	1.8	0.997
69.5	13.1	12.1	1.02	0.00275	0.5001	69.0	2.041	1.7	0.175	1.7	0.996
70.0	13.8	12.7	1.09	0.00212	0.504	69.5	2.157	1.6	0.183	1.6	0.996
70.8	13.2	12.1	1.03	0.00109	0.5098	70.3	2.029	1.7	0.173	1.7	0.996
71.4	13.1	12.1	1.03	0.00092	0.514	70.9	1.998	1.7	0.170	1.7	0.997
70.5	12.9	11.9	1.02	0.00093	0.508	70.0	2.010	1.7	0.170	1.7	0.997
70.3	13.1	12.1	1.04	0.00077	0.506	69.8	2.051	1.7	0.173	1.7	0.997
69.9	12.8	11.8	1.01	0.00104	0.503	69.4	2.000	1.7	0.170	1.7	0.998
71.0	13.8	12.7	1.09	0.00389	0.511	70.5	2.136	1.7	0.181	1.6	0.954
69.9	12.8	11.8	1.01	0.00089	0.503	69.4	2.005	1.7	0.170	1.7	0.998
70.9	13.3	12.3	1.04	0.00107	0.510	70.4	2.046	1.7	0.174	1.7	0.996
70.1	12.8	11.8	1.01	0.00285	0.505	69.6	1.997	1.7	0.170	1.7	0.997
70.8	12.5	11.5	0.96	0.00164	0.510	70.3	1.891	1.8	0.164	1.8	0.995
70.1	12.2	11.3	0.95	0.00136	0.504	69.6	1.876	1.8	0.162	1.8	0.997
70.2	11.9	11.0	0.92	0.00101	0.505	69.7	1.824	1.8	0.157	1.8	0.997
69.0	11.5	10.6	0.87	0.00264	0.497	68.5	1.752	1.9	0.155	1.9	0.993
70.6	11.6	10.7	0.87	0.00628	0.508	70.1	1.713	1.9	0.152	1.9	0.992
68.1	13.1	12.1	1.01	0.00237	0.491	67.6	2.068	1.7	0.179	1.7	0.994
69.5	12.1	11.1	0.92	0.00286	0.501	69.0	1.837	1.8	0.161	1.8	0.994
72.1	10.9	10.1	0.82	0.00150	0.519	71.6	1.580	2.0	0.141	2.0	0.995
69.4	11.0	10.1	0.83	0.00160	0.500	68.9	1.661	2.0	0.147	2.0	0.993
69.3	12.9	12.0	0.99	0.00120	0.499	68.8	1.984	2.0	0.174	2.0	0.993
70.4	10.9	10.1	0.80	0.00300	0.507	69.9	1.583	2.0	0.145	2.0	0.993
73.4	1.0	1.0	0.06	0.00436	0.529	72.9	0.119	19.6	0.013	19.6	1.000
72.4	1.2	1.2	0.06	0.00172	0.521	71.9	0.114	16.4	0.016	16.4	0.999
68.9	11.7	10.8	0.85	0.01054	0.496	68.4	1.712	1.9	0.158	1.9	0.991
70.5	11.1	10.3	0.82	0.00203	0.507	70.0	1.617	1.9	0.148	1.9	0.992
70.0	11.4	10.5	0.82	0.00160	0.504	69.5	1.632	1.9	0.152	1.9	0.992
69.6	11.8	11.0	0.87	0.00194	0.501	69.1	1.739	1.9	0.159	1.8	0.991
69.6	11.8	10.9	0.87	0.00140	0.501	69.1	1.733	1.9	0.158	1.8	0.991
70.4	10.9	10.1	0.80	0.00188	0.507	69.9	1.573	2.0	0.145	2.0	0.987
70.7	11.9	11.0	0.88	0.00181	0.509	70.2	1.722	1.9	0.157	1.8	0.986
70.8	10.8	10.0	0.79	0.00308	0.510	70.3	1.553	2.0	0.142	2.0	0.987
71.6	10.8	10.0	0.82	0.00401	0.515	71.1	1.585	2.0	0.141	2.0	0.992
70.6	10.9	10.1	0.80	0.00053	0.508	70.1	1.581	2.0	0.144	2.0	0.993
70.6	11.7	10.8	0.87	0.00061	0.508	70.1	1.720	1.9	0.154	1.9	0.993
70.7	10.4	9.6	0.78	0.00226	0.509	70.2	1.534	2.1	0.137	2.0	0.992
69.4	12.1	11.3	0.88	0.00054	0.500	68.9	1.766	1.8	0.163	1.8	0.991
72.5	8.0	7.4	0.58	0.00051	0.522	72.0	1.107	2.6	0.103	2.6	0.996
70.0	10.9	10.0	0.83	0.00090	0.504	69.5	1.651	2.0	0.144	2.0	0.994
70.2	13.2	12.3	0.97	0.00130	0.505	69.7	1.924	1.7	0.176	1.7	0.990
73.0	1.5	1.4	0.11	0.00544	0.525	72.4	0.203	13.3	0.019	13.3	0.999
71.8	1.8	1.6	0.13	0.00768	0.517	71.3	0.242	11.3	0.023	11.3	0.999
71.8	1.6	1.4	0.11	0.00556	0.517	71.3	0.210	12.9	0.020	12.9	0.999
71.5	8.6	8.0	0.55	0.00511	0.515	71.0	1.071	2.5	0.113	2.4	0.992
70.6	8.9	8.4	0.57	0.00399	0.509	70.1	1.126	2.4	0.119	2.3	0.991
72.7	8.0	7.5	0.51	0.01563	0.523	72.2	0.974	2.6	0.104	2.6	0.992

(continued on next page)

Table 1 (*continued*)

Sample	Spot No.	Mineral	$\delta^{18}O$ (‰)	$^{207}Pb/^{206}Pb$	Error % (1σ)	$^{208}Pb/^{206}Pb$	Error % (1σ)	$^{207}Pb/^{206}Pb$ Age (Ma)	Electron microprobe data[a]			
									UO_2	PbO	SiO_2	CaO
CS235m	4	uran	−22.0	0.06865	0.37	0.000736	3.5	888 ± 8	81.7	8.2	0.51	1.97
	5	uran	−24.8	0.06849	0.33	0.000522	4.2	884 ± 7	78.2	12.2	0.17	1.65
	6	uran	−23.7	0.06680	0.39	0.000990	3.1	831 ± 8	82.6	8.8	0.29	1.83
	7	uran	−27.0	0.06801	0.31	0.000724	3.1	869 ± 6	75.8	15.4	0.07	1.36
	8	uran	−25.0	0.07929	0.26	0.000235	4.9	1179 ± 5	78.9	11.4	0.49	1.54
	9	uran	−23.4	0.08709	0.22	0.000123	5.6	1362 ± 4	75.0	15.2	0.07	1.24
	10	uran	−26.4	0.06837	0.38	0.000529	5.1	880 ± 8	80.5	8.9	0.44	1.73
	11	uran	−32.3	0.06766	0.35	0.000496	3.9	858 ± 7	77.9	13.6	0.21	1.05
	12	uran	−23.3	0.06933	0.39	0.001034	4.2	909 ± 8	82.7	5.7	0.82	2.14
	13	uran	−26.1	0.06757	0.37	0.000763	3.5	856 ± 8	80.2	9.7	0.35	1.75

Spot locations for sample CS615A1 and CS235 m are shown in Figs. 6 and 7, respectively. Pb–Pb and U–Pb data for samples W83C and CS615A1 are from Fayek et al. (2000a). Abbreviations: uran = uraninite; coff = coffinite; Ca–U = calciouranoite; N.A = not available.

[a] All electron microprobe data are reported in units of wt.%. Uncertainty in measuring the Pb and U concentrations is ± 0.1 wt.% (100 ppm).

UO_2 were selected and arranged in clusters on double-sticky tape within a 25 mm-diameter brass mold. Buehler "Epoxide" epoxy resin was then poured in and allowed to harden overnight. The hardened epoxy mounts were separated from the brass moulds and polished using 600–2400 grit SiC sandpaper and, then, successively, 3 to 0.1 μm diamond polishing compounds. The mounts were then washed with a dilute soap solution, and rinsed in deionized water. The mounts were carbon coated and the individual grains examined for homogeneity by transmitted light microscopy, back scattered electron (BSE) imaging, and quantitative electron microprobe analysis.

Sections of core (25 mm in diameter) from the Cigar Lake unconformity-type uranium deposit, northern Saskatchewan, were similarly prepared for ion and electron microprobe analysis. Chemical compositions of the uraninite (Table 1) were determined by wavelength dispersive spectroscopy using an automated CAMECA 50 X-ray microanalyzer operated at 15 keV, a beam diameter of 10 μm, and counting times of 40 s per element. Synthetic UO_2 and minerals (grossular garnet for Si and Ca and galena for Pb) were used as standards. Detection limits of the elements (Table 1) were on the order of 0.1 wt.%. The program PAP was used to reduce the data for the various elements. Oxygen contents of uraninite were calculated by stochiometery assuming an ideal composition of UO_2. The mounts were placed in steel sample holders where surface conductivity was approximately 5–10 Ω/cm. The entire assembly was then placed in the ion microprobe sample lock and held at high vacuum for a minimum of 8 h prior to the start of analysis.

3.2. HRTEM analyses of uranium oxide minerals

Samples for HRTEM were prepared by slicing ~ 100 μm-thick portions of the probe mounts and selecting 3 mm-diameter chips from these sections. The chips were then polished on both sides using a lap grinder to an approximate thickness of 20–30 μm and then mounted onto a TEM sample copper disk. The samples were treated for 8–16 h in a rapid-etching ion-milling apparatus (6 keV, 2.5 mA, 15°–20° inclination) until perforated. The samples were then usually treated for 15–20 min at a 6°–10° inclination to clean the surface. Some samples were crushed and powdered, and the powders placed on carbon grids. Prepared samples were then examined using a JEOL JEM-2010 high-resolution transmission electron microscope (HRTEM). This instrument has analytical capabilities and a point-to-point resolution of 1.9 Å.

3.3. Conventional stable isotope analyses of the UO_2 standards

The oxygen isotopic composition of a synthetic uraninite crystal ($UO_{2.1}$) was isotopically characterized by conventional methods to calibrate it for potential use as an ion microprobe standard. Oxygen was liberated from multiple fractions of finely powdered

U (%)	Pb (%)	^{206}Pb	^{207}Pb	^{208}Pb	^{235}U	^{238}U	^{207}Pb/^{235}U	Error (%)	^{206}Pb/^{238}U	Error (%)	$\rho(x,y)$
72.0	7.6	7.1	0.49	0.00526	0.518	71.5	0.947	2.7	0.100	2.7	0.992
68.9	11.4	10.6	0.73	0.00555	0.496	68.4	1.466	1.9	0.155	1.9	0.987
72.7	8.1	7.6	0.51	0.00754	0.524	72.2	0.972	2.6	0.106	2.6	0.990
66.8	14.3	13.4	0.91	0.00970	0.481	66.3	1.894	1.6	0.202	1.6	0.984
69.5	10.6	9.8	0.78	0.00231	0.500	69.0	1.554	2.0	0.142	2.0	0.993
66.1	14.1	13.0	1.13	0.00159	0.476	65.6	2.369	1.6	0.197	1.6	0.992
70.9	8.2	7.7	0.53	0.00408	0.511	70.4	1.033	2.6	0.110	2.5	0.990
68.6	12.6	11.8	0.80	0.00587	0.494	68.1	1.621	1.8	0.174	1.7	0.983
72.8	5.3	5.0	0.35	0.00515	0.524	72.3	0.659	3.8	0.069	3.8	0.995
70.6	9.0	8.4	0.57	0.00642	0.509	70.1	1.118	2.4	0.120	2.3	0.989

(<350 μm) material derived from a single UO_2 crystal by using the BrF_5 technique of Clayton and Mayeda (1963). Oxygen isotopic compositions are reported in units of ‰ relative to Vienna Standard Mean Ocean Water (V-SMOW). Replicate analyses for $\delta^{18}O$ are reproducible to ± 0.1 ‰, and the $\delta^{18}O$ value of NIST-28 quartz is 9.6 ‰. The oxygen yield for UO_2 was 3.8 ± 0.3. Multiple measurements (5) gave a $\delta^{18}O$ value of 8.1 ± 0.3 ‰.

3.4. Ion microprobe oxygen isotopic analyses of synthetic UO_2 and uraninite

Isotopic analyses of the UO_2 standard and the unknown, uraninite, were made at UCLA with the CAMECA IMS 1270 ion microprobe (de Chambost et al., 1991) in multi-collection mode, by sputtering with a ~ 10 μm $\times$ 20 μm, 0.5-nA primary beam of Cs^+ ions with impact energy ~ 20 keV. This beam creates a crater depth of approximately 500 nm. Low energy (0 to 30 eV) negative secondary ions were analyzed. A mass resolving power ($M/\Delta M$) of ~ 2000 (full width at 10% full height) was sufficient to eliminate isobaric hydride interferences and generate flat peak tops ~ 0.020 amu wide for oxygen isotopes.

The recent development of the multicollector detection system for the CAMECA IMS 1270 SIMS has permitted routine high-resolution (~ 10 μm scale) high precision (sub per mil) in situ O isotopic analyses of geological materials (Fayek et al., 2001). The multicollector consists of five motorized, computer-controlled, movable collector units. Each unit can be configured to contain either an electron multiplier (EM) or Faraday cup (FC) with a slit assembly.

Secondary ion intensities are high enough to permit the detection of both major and minor isotopes of oxygen by Faraday cups (FC). Faraday cup precision is on the order of 10^{-4} A. A primary beam current of ~ 2.7 nA produced a $\sim 2 \times 10^9$ counts/s for ^{16}O and $\sim 6 \times 10^6$ for ^{18}O. The FC signals were measured by electrometers housed in a temperature-controlled vacuum chamber ($\sim 10^{-3}$ Torr) with feedback resistor of 10^9 Ω. Typically, drift in the FC detection system over a 12-h period was ~ 0.2 fA, or approximately 1 ‰ of the $^{18}O^-$ signal, and corrected for by making several FC background measurements during each day of analysis. Measurements comprised 25 cycles, each cycle consisting of a 10-s measurement. Internal precision of ± 0.3 ‰ under these conditions was routinely obtained for analyses of <5 min duration.

Fig. 2 shows ion microprobe oxygen isotopic analyses of different spots of the UO_2 standard made over a several-analyses session. The solid line in the plot represents the reference isotopic value determined by conventional methods, whereas the dashed lines represent the standard deviation calculated from the ion microprobe data. The data show some additional scatter beyond the internal precision; however, there is no trend within a single population with a standard deviation of 0.5 ‰ (Fig. 2). This value may be taken as representative of the overall point-to-point repro-

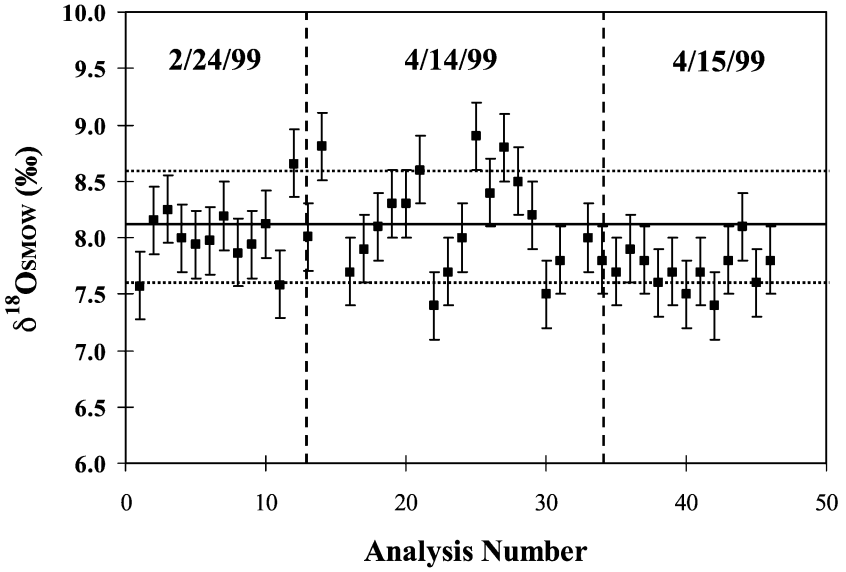

Fig. 2. External reproducibility of oxygen isotope analyses measured over a several analytical sessions for synthetic UO_2. Shown are mass-fractionation corrected $\delta^{18}O_{SMOW}$ values with 1σ error bars. Solid lines represent the accepted value based on conventional analyses. Data from Table 2.

ducibility of the method. Although the typical spot-to-spot reproducibility of $\sim \pm 0.5‰$ is not as precise as that obtained by conventional analyses, the amount of material consumed during ion microprobe analysis is generally about 10^5 times less providing us with a very high spatial resolution.

The oxygen isotopic composition of uranium minerals (i.e., coffinite and Ca-rich uranyl oxides) other than uraninite could not be measured by ion microprobe because a chemically and isotopically suitable standard was not available.

3.5. Data presentation and IMF correction

All oxygen isotopic data are presented using standard δ-notation relative to the appropriate standards, Vienna Standard Mean Ocean Water (V-SMOW) for $^{18}O/^{16}O$ and Vienna Peedee Belemnite (V-PDB) for $^{13}C/^{12}C$. The equation for calculating δ values in units of per mil (‰) is:

$$\delta_{\text{sample}} = (R_{\text{sample}} - R_{\text{std}})/R_{\text{std}} \times 10^3 \quad (1)$$

where R_{sample} and R_{std} are the absolute ratios in sample and standard, respectively. δ_{bias}, which is the isotope mass fractionation that occurs during SIMS analysis, was calculated in the same manner as δ_{sample}, using Eq. (1).

3.6. Ion microprobe Pb isotopic analyses of uranium oxides

The analytical protocol for uranium mineral U–Pb measurements using the CAMECA ims 1270 is similar to that used by Fayek et al. (2000a). A $\sim$ 1-nA primary ion beam of O^- was focused to a 15×30 μm spot. The following species were detected sequentially by switching the magnetic field: 203.5 (background), $^{204}Pb^+$, $^{206}Pb^+$, $^{207}Pb^+$, and $^{208}Pb^+$. High resolution mass scans indicate that isobaric interferences were fully resolved. A typical analysis lasted $\sim$ 10 min comprising of 25 analysis cycles. Common Pb ($^{204}Pb^+$) was not detected. Lead isotopic analyses of uranium oxide minerals by ion probe were made during separate analytical sessions on the same spots that were analyzed for their oxygen isotopic composition. Oxygen isotopic analyses preceded the analyses of Pb isotopes so that O^- primary beam used to obtain Pb isotopic data would not contaminate the analysis area. Instrumental mass fractionation due to matrix effects does not occur for the isotopes of lead in minerals (i.e., zircon, uraninite, etc.), therefore, a

standard was not required and obtaining the Pb isotopic composition of all the uranium-bearing minerals such as, uraninite, coffinite, and Ca-rich uranyl oxide was possible.

3.7. Calculation of U/Pb ratios

The Pb isotope ratios determined by ion microprobe and the concentration of Pb measured by electron probe from the same spot were combined to calculate the concentrations of ^{206}Pb and ^{207}Pb. Using the present-day ^{238}U/^{235}U ratio of 137.88 and the U concentration measured by electron probe, the amounts of ^{238}U and ^{235}U were calculated. The concentrations of ^{238}U, ^{235}U, ^{206}Pb, and ^{207}Pb were then used to calculate ^{206}Pb/^{238}U, and ^{207}Pb/^{235}U for each spot. This method avoids the need for a concordant uraninite or coffinite ion microprobe standard with homogenous U/Pb ratios because only the Pb isotopes are measured by ion microprobe, which exhibit negligible instrumental fractionation during sputtering (Meddaugh, 1983; Zetterström et al., submitted for publication).

3.8. Error calculation.

The uncertainties in the ^{206}Pb/^{238}U and ^{207}Pb/^{235}U ratios, σx and σy, respectively, and the covariance, σxy, were calculated by propagating the uncertainties in measuring Pb isotopic ratios by ion probe and the uncertainties in measuring the Pb and U concentrations by electron probe (Table 1). The largest source of error in this method is in the determination of U and Pb concentrations by electron microprobe. Concordia intersections were calculated using the program ISOPLOT (Ludwig, 1993). Uncertainties in the ages are 1σ in every case. Detailed error calculations equations used in calculating the isotopic ratios are presented in Fayek et al. (2000a).

4. Petrographic relations and mineral paragenesis

4.1. Uraninite

Uraninite at Cigar Lake occurs as black to dark grey masses with a metallic to sub-metallic luster. Uraninite is highly fractured, with sulfides, arsenides, clay, and rust-colored carbonate minerals (mainly calcite) infilling fractures. X-ray diffraction revealed uraninite, coffinite, galena, chalcopyrite, and pyrite as the most abundant minerals in the clay-free fraction of the ore (Janeczek and Ewing, 1994).

As with other uranium deposits in the Athabasca Basin, three main stages of ore formation were observed in thin section and by BSE. These are: stage 1 (U1), 2 (U2), and 3 uraninite (U3). All stages of uranium ore are variably altered to Ca–Si-rich, hydrous uranium minerals and coffinite. Stage 1, 2 and 3 uraninites occur as masses, uraninite cubes, and pseudo-cubes, ranging in size from 0.1 to 0.5 cm. Stage 1 and 2 uraninites occur as nodular masses that range in size up to 5 cm across. Nodules are composed of many botryoids that exhibit radial textures in thin section as a result of uniformly distributed radial shrinkage cracks. Spaces between botryoids of stage 1 uraninite are filled with clay minerals, Ni–Cu arsenides and Ni–Co sulf-arsenides (Reyx and Ruhlmann, 1993). However, Cu–Fe-sulfides are commonly associated with stage 3 uraninite (Bruneton, 1987; Reyx and Ruhlmann, 1993).

Stage 1 uraninite is characterized by high PbO contents (13.10 to 14.54 wt.%) and low SiO_2 and CaO contents (<1 wt.%); whereas, stage 2 uranium minerals are characterized by intermediate PbO contents (7.78 to 11.64 wt.%) and intermediate SiO_2 and CaO contents (1–3.5 wt.%), and stage 3 uraninite has low to moderate PbO contents (0.24 to 6.33 wt.%) and variable SiO_2 and CaO contents (Fayek et al., 1997a). However, all three stages of uraninite have high uranium contents (77.52 to 84.37 wt.%).

Stage 1 and 2 uraninites have similar X-ray powder-diffraction patterns which are consistent with UO_2 (Fayek et al., 2000b). Selected area diffraction and lattice images obtained using HRTEM of the least altered stage 1 and 2 uraninites show that these uraninite samples are well crystallized and essentially defect-free (Fig. 3a; Fayek et al., 2000b). The energy-dispersion spectroscopy (EDS) of these well-crystallized uraninite samples indicates that they have relatively high Pb contents but low Si and Ca contents (Fig. 3b; Fayek et al., 2000b). A more detailed description of the uranium ore can be found in Fayek et al. (1997a).

HRTEM analyses of stage 3 uraninite have identified patches of uraninite (~ 500 μm) and coffinite being replaced by a Ca-rich uranyl-oxide hydrate

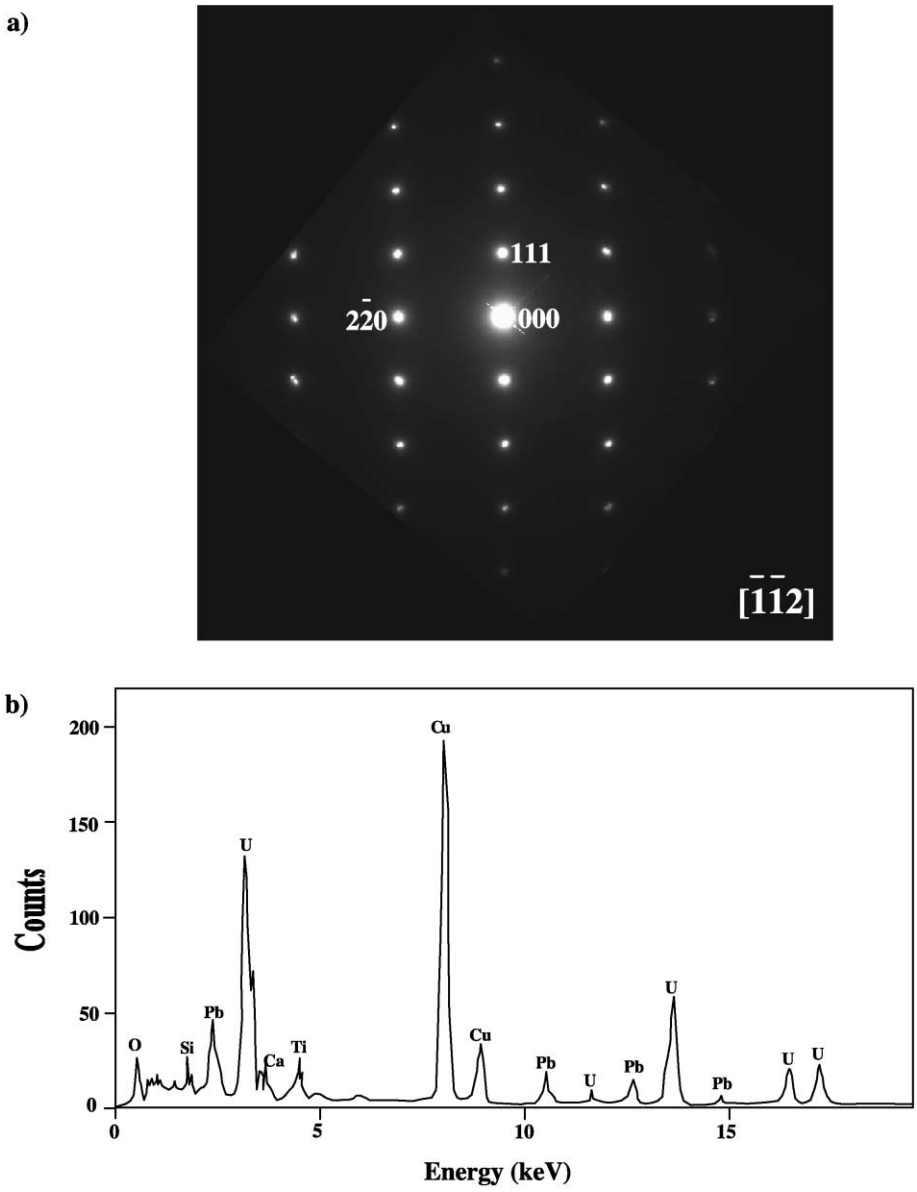

Fig. 3. (a) Selected area electron diffraction pattern of stage 1 uraninite (sample CS615A1); (b) energy dispersive spectrum (EDS) of stage 1 uraninite (sample CS615A1). The Cu is from the Cu grid.

mineral (Fig. 4a). Selected area diffraction patterns obtained by HRTEM show that this Ca-rich uranyl-oxide hydrate mineral is crystalline (Fig. 4b) and calculated *d*-spacings from selected area diffraction patterns indicate a unit cell that is distinctly different from that of uraninite, with the most intense diffraction peaks most closely matching those of calciouranoite ($CaU_2O_7{\cdot}5H_2O$) heated to 900 °C (see below; Table 2). However, the structure of calciouranoite is not known. In areas where the uraninite is partially altered to calciouranoite, lattice images (Fig. 4c) show a ''comb''-like texture that is probably the result of a volume change that occurs during the alteration process. Similar textures occur when biotite alters to chlo-

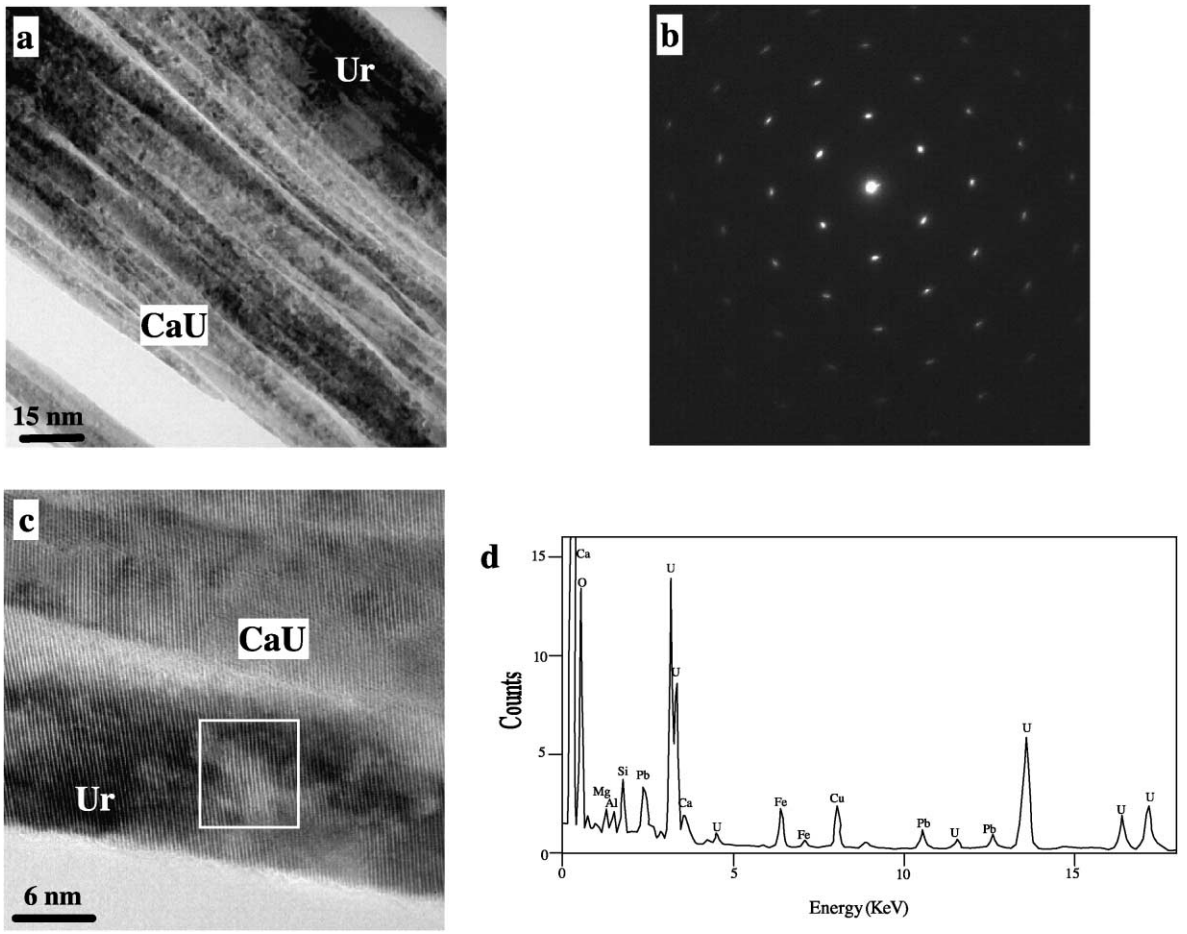

Fig. 4. (a) Bright field image of calciouranoite (CaU) with relict uraninite (Ur); (b) selected-area diffraction pattern showing the crystalline nature of calciouranoite; (c) high-resolution transmission electron (HRTEM) image showing relic uraninite (Ur) and calciouranoite (CaU), and the "comb" texture (white box) associated with volume change during the alteration of uraninite to calciouranoite; (d) energy dispersive spectrum (EDS) of calciouranoite (Sample CS235 m). The Cu is from the Cu grid.

rite (Baronnet, 1992; Veblen, 1992). Uraninite-free regions are characterized by high Ca contents and relatively low to moderate Si and Pb contents (Fig. 4d).

4.2. Coffinite

Coffinite, in hand specimen, occurs as grey-black microveinlets. In thin section, coffinite occurs as colliform bands along uraninite grains and botryoids and as feathery crystalline dark grey masses in carbonate veins. Replacement of uraninite and by coffinite was pervasive along fractures and uraninite-sulfide contacts. Fine-grained coffinite often contains relics of uraninite (Fig. 5a) and is intimately intergrown with clays. Coffinite is characterized by low PbO contents (0 to 2.08 wt.%), moderate but variable CaO (0.42 to 4.94 wt.%) and occasionally low SiO_2 contents (9.00 to 18.41 wt.%; Fayek et al., 1997a).

Selected-area diffraction patterns of coffinite often show streaking (Fig. 5b) and concentric diffraction rings (Fayek et al., 2000b). High-resolution images reveal uraninite sub-grains (Fig. 5c), edge dislocations, low-angle grain boundaries, "bent" lattice fringes, and interstitial regions (Fig. 5c) that are characterized by relatively high Si and Ca contents (Fig. 5d) and variable Pb contents. Similar features are observed in

Table 2
Interplanar spacing for uraninite, coffinite and calciouranoite from the Cigar Lake unconformity-type uranium deposit

Uraninite					Coffinite					Calciouranoite		
(JCDPS #20-1344)[a]			(CS 615 220)		(JCPDS #11-420)			(CS 235L 113)		(Rogova et al., 1974a)[b]		(CS 235 L 113)
d(*A*)	Int.	*hkl*	*d*(*A*)[c]	*hkl*	*d*(*A*)	Int.	*hkl*	*d*(*A*)	*hkl*	*d*(*A*)	Int.	*d*(*A*)
3.140	100	111	3.11	111	4.640	95	101	4.76	101	5.741	40	
2.721	45	200	2.73	200	3.480	100	200	3.54	200	3.367	60	
1.924	50	220	1.94	220	2.789	45	211			3.206	90	3.23
1.641	50	311			2.636	95	112			2.720	60	2.79
					1.803	70	312			2.460	40	
										1.974	90	
										1.880	50	
										1.850	50	
										1.776	50	
										1.685	40	
										1.684	90	1.62
										1.600	40	
										1.563	40	
										1.452	40	
										1.394	40	1.40
										1.349	50	
										1.286	40	
										1.176	40	
										1.152	40	
										1.142	40	
										1.117	70	
										1.064	60	1.06
										1.044	70	
										1.006	60	
										0.996	60	

[a] JCPDS-ICDD copyright (c) 1990.
[b] *hkl* values are unavailable because unit cell is not known.
[c] *d*-spacing of most intense peaks (>40%) from electron diffraction patterns.

samples from Oklo, Gabon and are interpreted to be the result of radiation damage, despite the relatively rapid annealing of radiation-induced defects in uraninite (Casas et al., 1998).

The close association of sulfides, such as chalcopyrite, with coffinite suggests that coffinite formed under reducing conditions ($fO_2 < 10^{-40}$) (Janeczek and Ewing, 1992). Coffinite is stable relative to uraninite at intermediate dissolved silica levels ($\sim 10^{-4}$ to 10^{-3} mol/l; (Langmuir, 1978)). In fluids permeating through the sandstone, the dissolved silica concentrations reach 5.1×10^{-4} mol/l (Janeczek and Ewing, 1992). Therefore, it is not surprising that extensive coffinitization occurs at Cigar Lake. However, the P–T conditions for coffinite formation are not well defined (Janeczek and Ewing, 1992). The thermal stability of coffinite has been reported to range between 25 °C and 1000 °C (Hoekstra and Fuchs, 1956; Hemingway, 1982).

4.3. Ca-uranyl-oxide hydrate minerals

In hand specimen, uranyl-oxide hydrate minerals are yellow to orange in color and occur as microveinlets that cut across uraninite. In thin section, uranyl minerals are closely associated with coffinite and occur as homogenous colliform bands along the edges of uraninite grains or as microveinlets that cut across the common uranium ore minerals (Fayek et al., 1997a). These minerals are characterized by low UO_2 contents (63.1 to 82.50 wt.%), variable PbO contents (<0.1 to 12.17 wt.%), and intermediate to low SiO_2 and CaO contents (0.18 to 6.49 wt.%). However, there is no correlation between UO_2 and PbO contents

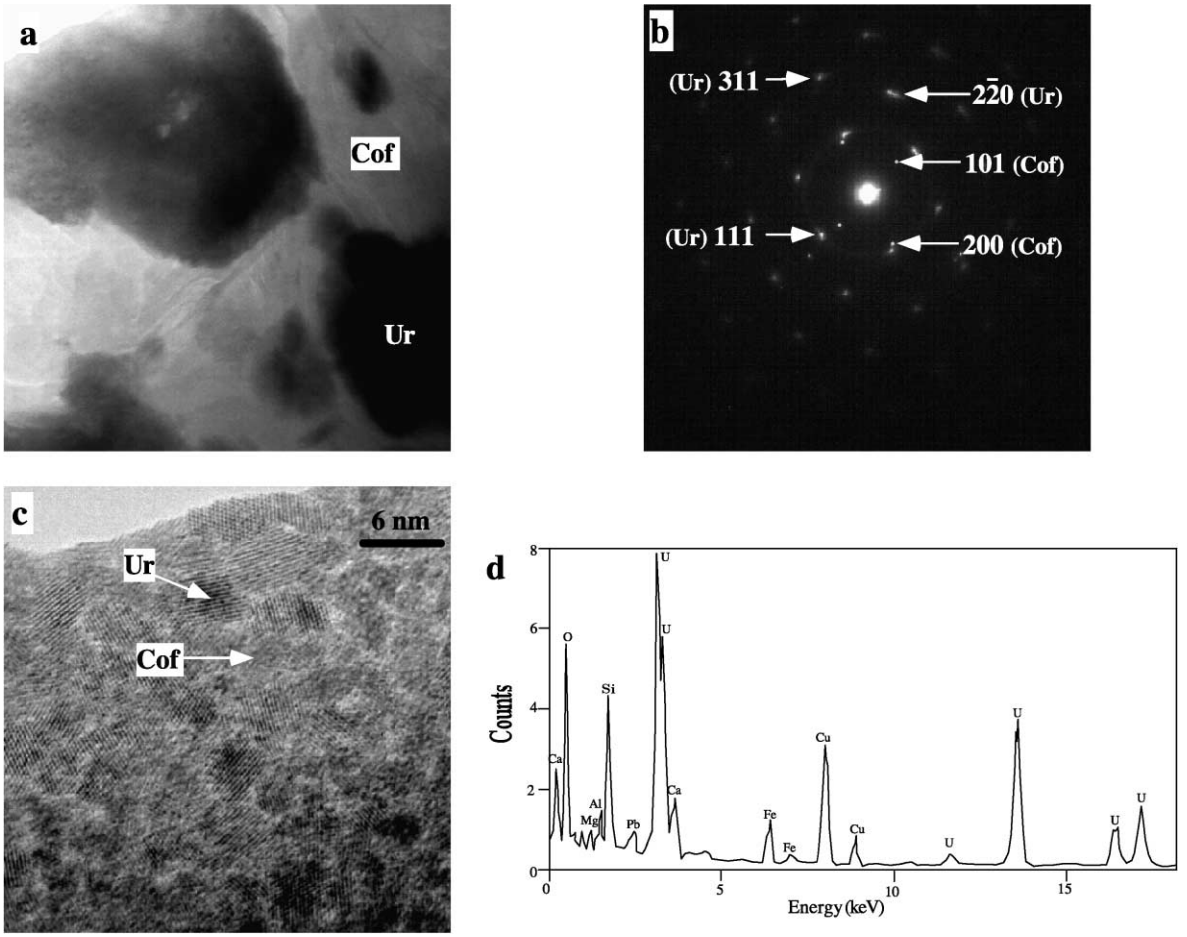

Fig. 5. (a) Bright-field image of coffinite (Cof) with relict uraninite (Ur); (b) selected area diffraction pattern showing two phases: uraninite and coffinite; (c) high-resolution transmission electron (HRTEM) image showing bent lattice fringes and polycrystalline microtexture. Subgrains are uraninite (Ur) with interstitial coffinite zones (Cof); (d) energy dispersive spectrum (EDS) of coffinite rich zones (Sample CS235 m). The Cu is from the Cu grid.

of uranyl oxide hydrate-uraninite alteration minerals (Fayek et al., 1997a).

The uranyl minerals could not be identified based on the X-ray powder-diffraction pattern because they are fine grained (<15 nm). However, HRTEM analyses of stage 3 uraninite and calculated *d*-spacings from selected area diffraction patterns indicate that the Ca-rich uranyl mineral is likely calciouranoite (Fig. 4; Table 2).

Calciouranoite was first described by Rogova et al. (1974a) as a higher hydrate of metacalciouranoite (Rogova et al., 1974b). Calciouranoite occurs generally as a brownish-orange poorly crystalline coating that must be heated to produce a powder X-ray diffraction pattern and can be represented ideally by the formula $CaU_2O_7{\cdot}5H_2O$. Electron microprobe analyses by Rogova et al. (1974a) show that calciouranoite has moderate UO_2 contents (68.02 to 71.78 wt.%), low PbO contents (1.18 to 2.68 wt.%), and low to moderate SiO_2 (0.32 to 4.00 wt.%) and CaO contents (5.86 to 6.77 wt.%), which are similar in composition to the calciouranoite from Cigar Lake (Fayek et al., 1997a). However, the calciouranoite from Cigar Lake has higher PbO contents because it replaces a Proterozoic uraninite ($\sim$ 1500 Ma), which has a high PbO content relative to that of the upper

Jurassic to lower Cretaceous uraninite that was studied by Rogova et al. (1974a,b).

Published studies on the dissolution, oxidation, and secondary phase formation during the interaction between uraninite and UO_2- and silica-saturated oxidizing fluids have shown that shortly after the onset of uraninite or UO_2 dissolution, uranyl-oxide hydrates (e.g. becquerelite and curite) precipitate followed by uranyl-silicate minerals such as soddyite and uranophane and eventually uranyl alkali silicates (Finch and Ewing, 1992; Fayek et al., 1997b). Therefore, the close association between coffinite and calciouranoite and moderate Si contents of calciouranoite suggests that in the presence of oxidizing fluids coffinite may alter to higher oxide hydrate phases.

5. Oxygen isotope systematics

Previously reported $\delta^{18}O$ values of stage 1, 2 and 3 uraninites from Cigar Lake (-28.5 to -3.8‰; Fayek et al., 1997a), which were obtained by micro-drilling thick sections and analysing the powders by the fluorination technique, show a wide range of values with generally increasing $\delta^{18}O$ values with increasing SiO_2 and CaO contents and with each subsequent stage of uraninite. However, it was not clear whether the increase in $\delta^{18}O$ values with increasing SiO_2 and CaO contents was the result of uraninite precipitating from subsequent fluids with higher SiO_2 and CaO contents or incorporation of Si- and Ca-rich minerals, such as clays, coffinite, and Ca-uranyl-oxide hydrates, during the micro-drilling procedure. The high spatial resolution of the in situ oxygen isotopic measurements by ion microprobe (15×30 μm) has allowed us to analyse relatively unaltered regions of uraninite, devoid of alteration minerals, within a single thin section. Figs. 6 and 7 show back-scattered electron images of stage 1, 2 and 3 uraninites, respectively, and the spots analysed by electron and ion microprobe. Ion microprobe $\delta^{18}O$ measurements obtained from 20 to 100 μm areas of stage 1, 2 and 3 uraninites indicate that portions of the uraninite inferred petrologically to be relatively unaltered have a range of $\delta^{18}O$ values from -33.9 to -20.5‰ (Fig. 8a). These values are among the lowest reported from unconformity-type uranium deposits from the Athabasca Basin. The exceptionally low and narrow range of $\delta^{18}O$ values obtained by ion microprobe relative to the analyses obtained by micro-drilling and conventional fluorination analyses confirms that even mm-scale sampling is insufficient to avoid veins of isotopically heavier, Ca–U oxide hydrates and coffinite. Electron microprobe analyses of the same spots analyzed by ion microprobe show that stage 2 and 3 uraninites have slightly higher SiO_2 and CaO content relative to stage 1 uraninite (Fig. 8b); however, this slight increase in SiO_2 and CaO content has had little effect on the $\delta^{18}O$ values of the uraninites.

Isotopic and microthermometric studies on clay, and silicate minerals in textural equilibrium with uraninite

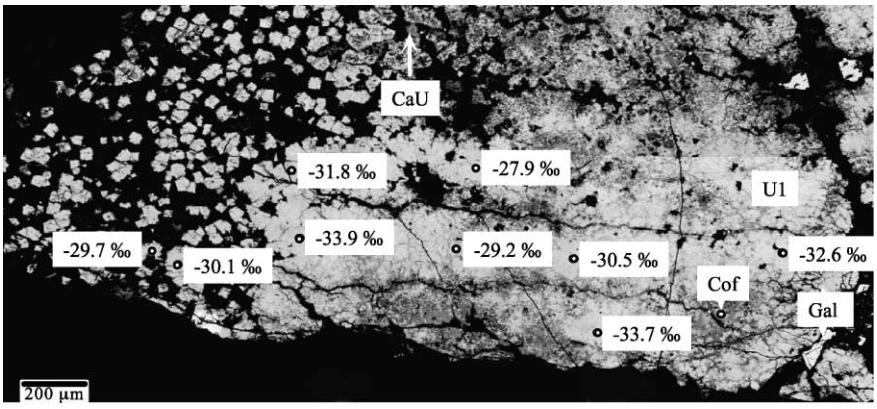

Fig. 6. Back-scattered electron image of stage 1 uraninite from Cigar Lake (CS615A1). Coffinite (Cof) and calciouranoite (CaU) alteration appears as dark gray while uraninite (U1) and galena (Gal) is light gray. Labeled spots indicate analyses points for U–Pb and O isotopic measurements.

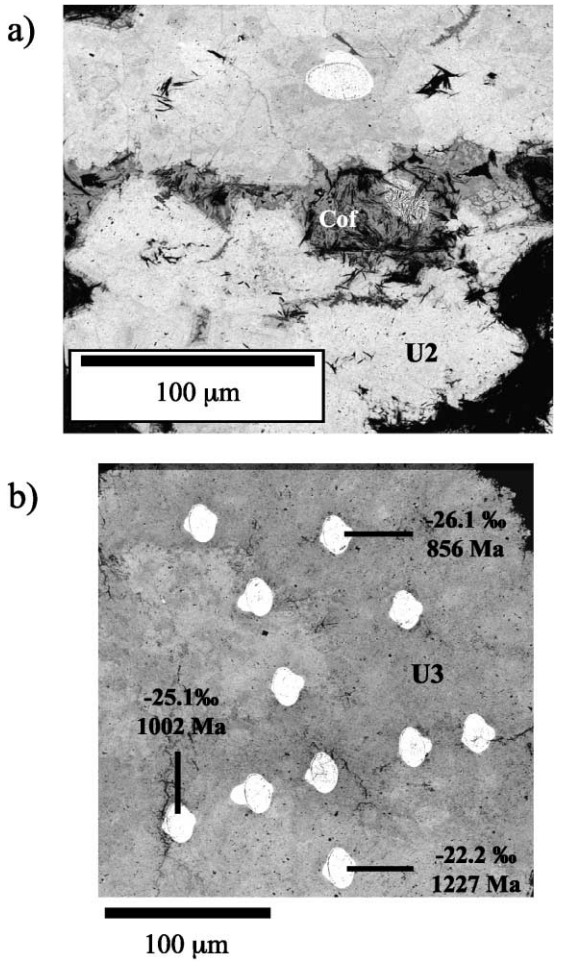

Fig. 7. Back-scattered electron image of (a) stage 2 uraninite (CS615B1). Coffinite (Cof) alteration appears as dark gray while uraninite (U2) is light gray. Also shown are two oval-shaped craters (very light gray) that mark spots that were analyzed by ion and electron microprobe; (b) stage 3 uraninite (CS235 m). Uraninite (U3) has a mottled texture where bright patches represent remnant stage 1 uraninite that was not completely recrystallized. Also shown are two oval-shaped craters (very light gray) that mark spots that were analyzed by ion and electron microprobe.

from the Cigar Lake and other unconformity-type uranium deposits from the Athabasca Basin indicate that the dominant fluids involved in the formation of unconformity-type uranium deposits were saline fluids having $\delta^{18}O$ values of approximately 4 ± 4 ‰ and temperatures of 175 ± 25 °C (e.g., Kotzer and Kyser, 1995). Using these results, in conjunction with theoretical and experimental uraninite-water fractionation factors (Hattori and Halas, 1982; Zheng, 1995; Fayek and Kyser, 2000), uraninite should have $\delta^{18}O$ values near -10 ‰. However, at temperatures of 200 °C, the $\delta^{18}O$ values of the uraninite indicate that they should have been in equilibrium with fluids with $\delta^{18}O$ values near -20 ‰. The fractionation between uraninite and water at temperatures $\sim 100-200$ °C is ~ 11 ‰ (Fayek and Kyser, 2000), and so the anomalously low $\delta^{18}O$ values of all three stages of uraninite are likely due to recrystallization of uraninite by late meteoric waters, which in the Athabasca area have $\delta^{18}O$ values of approximately -20 to -16 ‰ (Kotzer and Kyser, 1995), resulting in only minor disturbances to their chemical composition and texture, and limited actinide migration. This implies that these fluids were relatively reducing because uranium mineral chemistry and solubility is largely a function of fO_2 and uraninite is stable only under very reducing conditions ($fO_2 < 10^{-25}$; Cramer, 1995). Therefore, in situ oxygen isotopic analyses of uraninite not only can provide information regarding the fluid history of this deposit, but can also provide the base-line context for the interpretation of U mobilization during repository relevant time periods.

6. Pb–Pb and U–Pb isotope systematics

The $^{207}Pb/^{206}Pb$ ages of uraninite, coffinite and Ca-rich uranyl oxide minerals range from 254 to 1362 Ma. Samples of stage 1 uraninite tend to have homogenous $^{207}Pb/^{206}Pb$ ages, on the scale of the thin section, ranging from 1362 to 1222 Ma, whereas stage 2 and 3 uraninites predominantly have $^{207}Pb/^{206}Pb$ ages ranging from 1191 to 1140 Ma and 909 to 802 Ma, respectively. These ages are similar to those previously reported for uraninite from the Athabasca basin (e.g., Cumming and Krstic, 1992; Kotzer and Kyser, 1993; Fayek and Kyser, 1997). However, samples of stage 2 and 3 uraninites are generally less uniform in terms of their Pb isotopic composition, containing regions that give $^{207}Pb/^{206}Pb$ ages that are consistent with all three stages of uraninite (Fig. 8a). For example, $^{207}Pb/^{206}Pb$ ages from brighter regions observed in BSE images of stage 2 and 3 uraninites generally give ages that are consistent with stage 1 uraninite (Fig. 8a). These regions are interpreted to be remnant grains of stage 1 uraninite that were not

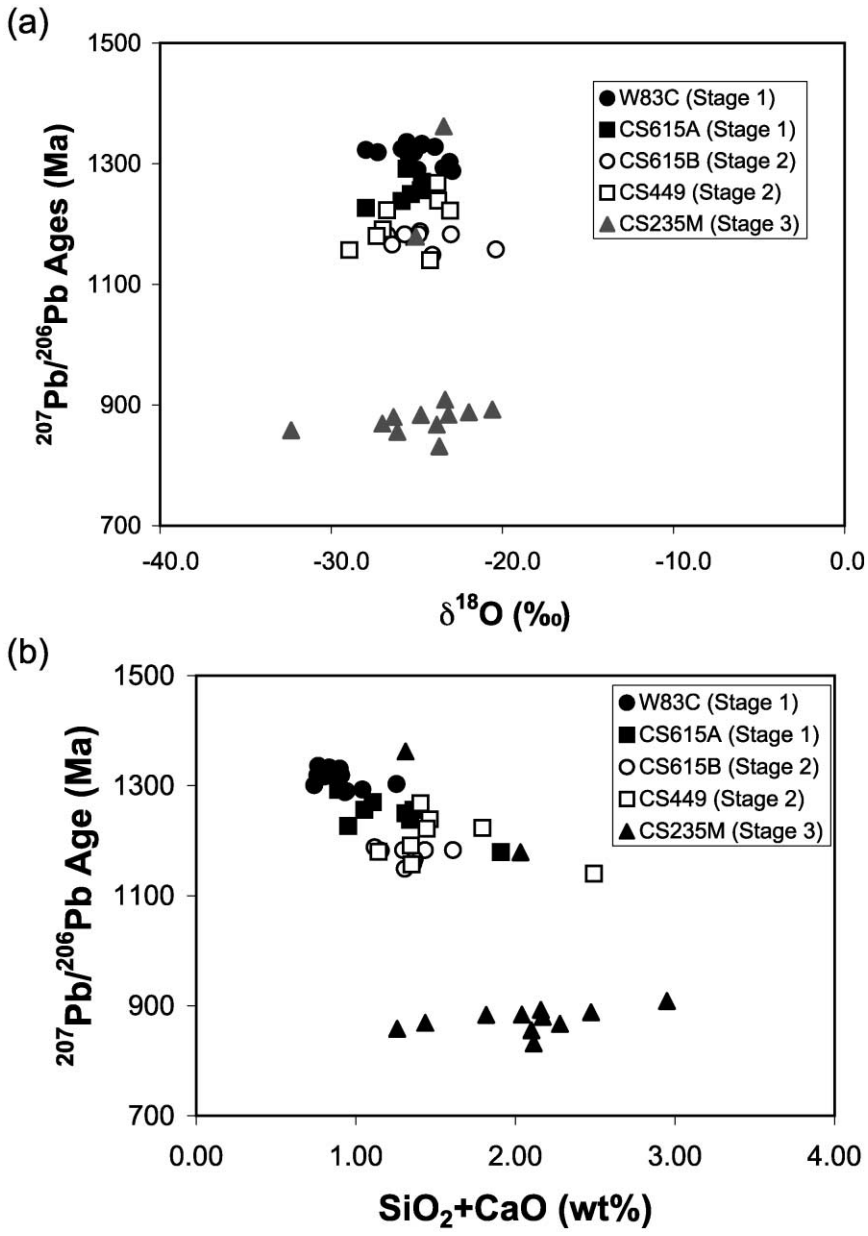

Fig. 8. Relationship between $^{207}Pb/^{206}Pb$ ages and (a) $\delta^{18}O$ values, and (b) $SiO_2 + CaO$ contents for three stages of uraninite from the Cigar Lake deposit. Data from Table 1.

completely overprinted by subsequent fluids that precipitated younger generations of uranium-bearing minerals. Ion microprobe analyses spots that overlap two stages of uraninite, within a single thin section, generally give intermediate $^{207}Pb/^{206}Pb$ ages (Fig. 7). The composite nature of stage 2 and 3 uraninites suggests that subsequent fluids have recrystallized older generations of uraninite and precipitated new uraninite, therefore, partially resetting the Pb isotope systematics of uraninite.

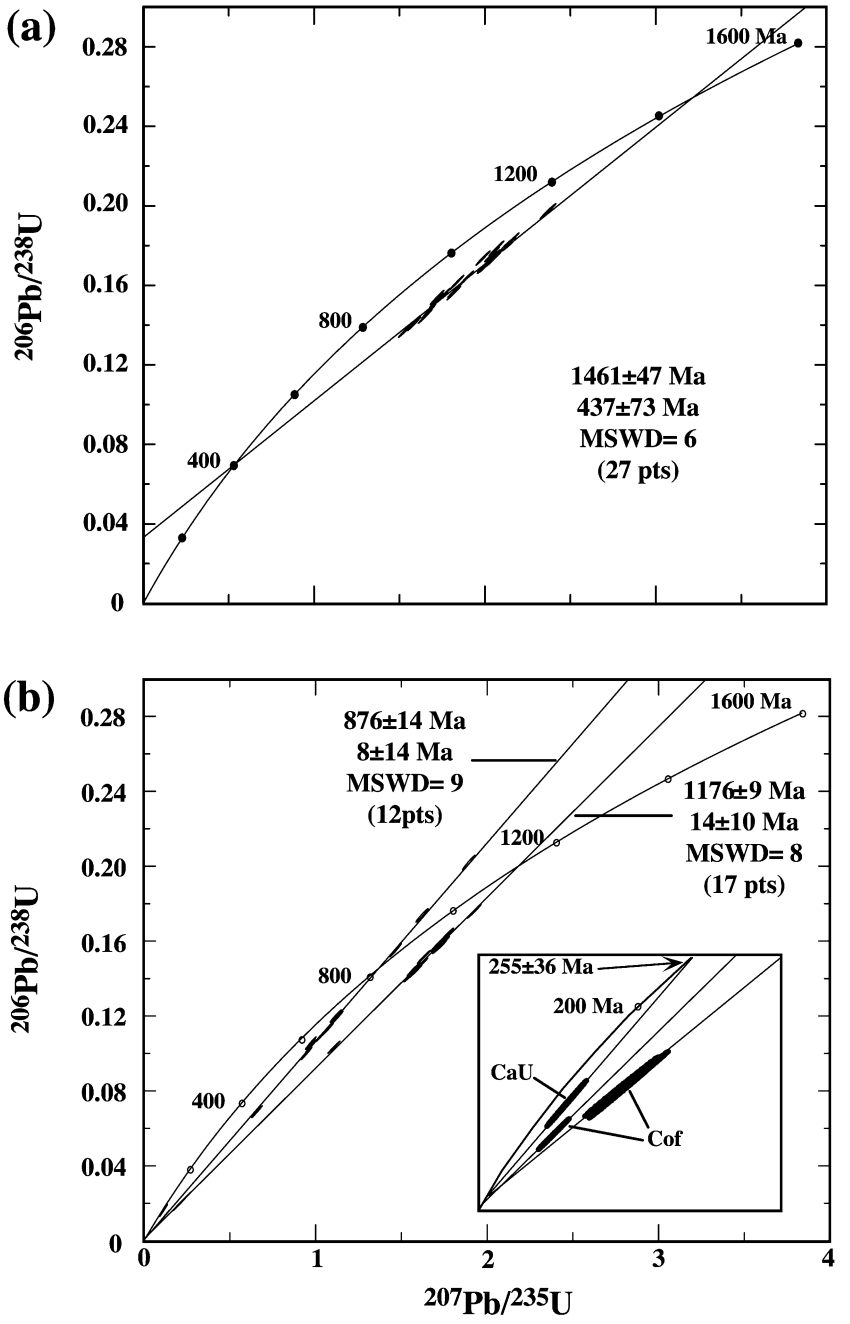

Fig. 9. (a) U–Pb results from in situ isotopic analyses of stage 1 uraninite from Cigar Lake. Some of the analysis points are identified in Fig. 6 and the data is reported in Table 1. (b) U–Pb results from in situ isotopic analyses of stage 2 and 3 uraninites, coffinite and calciouranoite from Cigar Lake. Some of the analysis points are identified in Fig. 7 and the data is reported in Table 1. Inset shows the lower portion of Concordia illustration three generations of secondary uranium minerals.

Si- and Ca-rich uranium minerals, such as coffinite and caclioуranoite, are associated with each stage of uraninite. Coffinite has $^{207}Pb/^{206}Pb$ ages of 1119–1082 and 802 Ma, whereas calciouranoite gives an age of 245 Ma. These ages suggest that there were several generations of Si- and Ca-rich alteration minerals, precipitating from Si- and Ca-rich fluids. The $^{207}Pb/^{206}Pb$ ages from coffinite are similar to the $^{207}Pb/^{206}Pb$ ages from stage 2 and 3 uraninites suggesting that these Si- and Ca-rich fluids were involved in the precipitation of stage 2 and 3 uraninites, which also tend to have higher Si and Ca contents relative to stage 1 uraninite (Fig. 8b).

Fig. 9a shows a concordia plot of the U–Pb data from stage 1 uraninite. When all 27 points are regressed together, an upper intercept of 1461 ± 47 Ma and lower intercept of 437 ± 73 Ma is obtained with an MSWD of 6. The age obtained from the regression of all the points is interpreted to represent the minimum age of mineralization, which corresponds with the Rb–Sr age of clay mineral alteration ($\sim$ 1477 Ma) associated with the unconformity-type uranium deposits (Kotzer and Kyser, 1995) and the age of one of the magnetization events (B-type magnetization, 1600–1450 Ma) from the Athabasca basin (Kotzer et al., 1992).

Fig. 9b shows a concordia plot of the U–Pb data from stage 2 and 3 uraninites, coffinite, and calciouranoite. Regression of the points, including two generations of coffinite, give upper intercepts of 1176 ± 9 and 876 ± 14 Ma, and lower intercept of 14 ± 10 and 8 ± 14 Ma, respectively. The ages obtained from the regression are also interpreted to represent the minimum age of mineralization. These ages correspond with the age of the Grenvillian Orgeny ($\sim$ 1100 Ma; Mallard and Rogers, 1997), which occurred to the southeast of the Athabasca Basin, and the age of one of the magnetization events (C-type magnetization, $\sim$ 900 Ma) from the Athabasca basin (Kotzer et al., 1992), which is likely due to fluids that migrated during the break up of Rhodinia (i.e., separation of North America from Australia at $\sim$ 900 Ma) (Young, 1992; Li et al., 1996).

Lead diffusion in uraninite is a rapid process with diffusion rates of three to six orders of magnitude faster than in silicates such as zircon (Yershov, 1974; Janeczek and Ewing, 1995). Therefore, the lower intercepts (e.g., 437 ± 73 Ma) likely do not reflect a Pb resetting event, but result from continuous Pb diffusion (Tilton, 1960). This continuous Pb diffusion model is plausible because the temperature remained relatively constant (below 200 °C) throughout the history of these deposits (Kotzer and Kyser, 1995).

Several of the points from stage 3 uraninite plot above concordia. These data are from samples that contain fine intergrowths of calciouranoite and generally have low uranium contents (Table 1). The presence of a uranyl oxide hydrate mineral, such as calciouranoite, indicates that uraninite has been hydrated and partially oxidized in the presence of a fluid. The low UO_2 contents are likely the result of the increased solubility of oxidized uranium and the preferential leaching of U^{6+} from uraninite. The age of the calciouranoite does not correspond with the uraninite or coffinite ages and is interpreted to be the result of late fluids that altered uraninite and coffinite.

In contrast, the concordia plot of data from Cigar Lake obtained by micro-drilling and conventional wet chemical techniques (Cumming and Krstic, 1992) shows a great deal of scatter. In their study, Cumming and Krstic (1992) were unable to avoid micrometer intergrowths of galena and coffinite. Therefore, the in situ U–Pb data analyses may be indicating the timing and nature of the recrystallizing event, which prior to the in situ analyses was obscured by the wide variability in the data obtained by micro-drilling and conventional isotopic analyses.

7. Conclusions

(1) We used a technique that utilizes both the electron and ion microprobe to obtain rapid and precise in situ U–Pb isotopic analyses of uranium minerals. The advantages of this technique over conventional methods and previous ion microprobe techniques are: (1) mineral separation and chemical digestion are not required, (2) a uranium mineral standard with homogenous Pb*/U is not required, and (3) minor alteration phase, such as coffinite, and calciouranoite with a complex chemistry can be routinely analyzed for their U–Pb isotopic composition.

(2) A concordia plot of U–Pb data, obtained by this technique, from three stages of uraninite and coffinite from the Cigar Lake uranium deposit are discordant with upper intercepts of 1461 ± 47, 1176 ± 9, and

876 ± 14 Ma. These ages correspond with the age of the clay mineral alteration associated with unconformity-type uranium deposits, ages of magnetization events from the Athabasca basin, and the Grenvillian Orogeny.

(3) Ion microprobe analysis by ion microprobe in multi-collection mode permits rapid (i.e. time per analyses <5 min), precise (± 0.5 ‰) in situ oxygen isotopic analysis of uraninite. The oxygen isotopic analyses of uraninite represent the first in situ stable isotopic measurements of uranium oxides.

(4) In situ oxygen isotopic analyses of discreet 20–100 μm size regions of uraninite, from the Cigar Lake Deposit, that appear to be free of alteration have the lowest $\delta^{18}O$ values (−33.9 to −20.4 ‰) ever reported for unconformity-type uranium deposits. These results suggest that uraninite likely interacted with fluids with $\delta^{18}O$ values of ca. −18 ‰, (i.e. similar in composition to recent meteoric waters) resulting in only minor disturbances to their chemical composition and texture, and limited actinide migration.

(5) The in situ technique, when applied to other deposits, can potentially help constrain the chronological and fluid evolution of unconformity-type uranium deposits. Chemical and isotopic characterizing of natural phases such as uraninite, coffinite, and calciouranoite provides an approach to confronting the long-term behavior of radioactive waste (i.e. UO_2 in spent fuel) in specific geologic environments. Determining the corrosion and behavior of radioactive waste by using natural analogue phases provides fundamental data that are significant to performance assessments of the waste over extended time periods.

Acknowledgements

This study was supported by a grant from the U.S. Department of Energy. We thank Dr. T.K. Kyser for providing the UO_2 standard and the facilities for conventional isotopic analyses. Kerry Klassen and Aliona Valyashko expertly provided technical assistance. We also thank Drs. Frank Kyte and Kevin McKeegan for their expert technical assistance. The UCLA ion microprobe laboratory is partially supported by a grant from the National Science Foundation Instrumentation and Facilities program. The manuscript greatly benefited from the constructive comments of Prof. Roberta Rudnick and the two referees who reviewed this manuscript.

References

Baronnet, A., 1992. Polytypism and stacking disorder. In: Buseck, P.R. (Ed.), Minerals and Reactions at the Atomic Scale: Transmission Electron Microscopy. Rev. Mineral., vol. 27. Mineralogical Society of America, Chelsea, MI, pp. 231–289.

Bruneton, P., 1987. Geology of the Cigar Lake uranium deposit (Saskatchewan, Canada). In: Gilboy, C.F., Vigrass, L.W. (Eds.), Economic Minerals of Saskatchewan. Sask. Geol. Soc. Spec. Publ., vol. 8, pp. 99–119.

Bruno, J., Casas, I., Puigdomènech, I., 1991. The kinetics of UO_2 under reducing conditions and the influence of an oxidized surface layer (UO_{2+x}): application of a continuous flow-through reactor. Geochim. Cosmochim. Acta 55, 647–658.

Bruno, J., DePablo, J., Duro, L., Figuerola, E., 1995. Experimental study and modeling of the U(VI)–FE(OH)(3) surface precipitation coprecipitation equilibria. Geochim. Cosmochim. Acta 59, 4113–4123.

Burns, P.C., Miller, M.L., Ewing, R.C., 1996. U^{6+} minerals and inorganic phases: a comparison and hierarchy of crystal structures. Can. Mineral. 34, 845–880.

Casas, I., de Pablo, J., Giménez, I., Torrero, M.E., Bruno, J., Cera, E., Finch, R.J., Ewing, R.C., 1998. The role of pe, pH, and carbonate on the solubility of UO_2 and uraninite under nominally reducing conditions. Geochim. Cosmochim. Acta 62, 2223–2231.

Clayton, R., Mayeda, T.K., 1963. The use of bromine pentafluoride in the extraction of oxygen from oxides and silicates for isotopic analysis. Geochim. Cosmochim. Acta 27, 43–52.

Cramer, J.J., 1995. The Cigar Lake uranium deposit: analogue information for Canada's nuclear fuel waste disposal concept. AECL Rep. 11204, 32 pp.

Cumming, G.L., Krstic, D., 1992. The age of unconformity-related uranium mineralization in the Athabasca Basin, northern Saskatchewan. Can. J. Earth Sci. 29, 1623–1639.

de Chambost, E., Hillion, F., Rasser, B., Migeon, H.N., 1991. The CAMECA ims 1270: a description of the secondary ion optical system. In: Benninghoven, H. (Ed.), SIMS VIII Proceedings. Wiley, New York, pp. 207–210.

Dyck, W., 1978. The mobility and concentration of uranium and its decay products in temperate surficial environments. In: Kimberley, M.M. (Ed.), Short Course in Uranium Deposits: Their Mineralogy and Origin. Mineral. Assoc. Can., vol. 3, pp. 57–92.

Fayek, M., Kyser, T.K., 1997. Characterization of multiple fluid events and Rare-Earth-Element mobility associated with formation of unconformity-type uranium deposits in the Athabasca Basin, Saskatchewan. Can. Min. 35, 627–658.

Fayek, M., Kyser, T.K., 2000. Low temperature oxygen isotopic fractionation in the uraninite–UO_2–CO_2–H_2O system. Geochim. Cosmochim. Acta 64, 2185–2197.

Fayek, M., Janeczek, J., Ewing, P.C., 1997a. Mineral chemistry and oxygen isotopic analyses of uraninite, pitchblende and uranium

alteration minerals from the Cigar Lake deposit, Saskatchewan, Canada. Appl. Geochem. 12, 549–565.

Fayek, M., Kyser, T.K., Ewing, R.C., Miller, M.L., 1997b. Uraninite–water interaction in an oxidizing environment. Mater. Res. Soc. Symp. Proc. 465, 1201–1208.

Fayek, M., Harrison, T.M., Grove, M., Coath, C.D., 2000a. A rapid in situ method for determining the ages of uranium oxide minerals. Int. Geol. Rev. 42, 163–171.

Fayek, M., Burns, P.C., Guo, Y.-X., Ewing, R.C., 2000b. Microstructures associated with uraninite alteration. J. Nucl. Mater. 277, 204–210.

Fayek, M., Harrison, T.M., Grove, M., Coath, C.D., Ewing, R.C., 2001. In situ stable isotopic analyses of multiple generations of cementation associated with a petroleum reservoir, North Coles Levee, San Joaquin Basin, California. J. Sediment. Res. 71, 444–485.

Finch, R.J., Ewing, R.C., 1992. Corrosion of uraninite under oxidizing conditions. J. Nucl. Mater. 190, 133–156.

Goodwin, B.W., Cramer, J.J., McConnel, D.B., 1988. The role of natural analogues in performance assessment. IAEA Technical Report Series: Appendix B, pp. 37–45.

Grandstaff, D.E., 1976. A kinetic study of the dissolution of uraninite. Econ. Geol. 71, 1493–1506.

Hattori, K., Halas, S., 1982. Calculation of oxygen isotope fractionation between uranium dioxide, uranium trioxide and water. Geochim. Cosmochim. Acta 46, 1863–1868.

Hemingway, B.S., 1982. Thermodynamic properties of selected uranium compounds and aqueous species at 298.15 K and 1 bar and at higher temperatures—preliminary models for the origin of coffinite deposits. U.S.G.S. Open-file Rep, pp. 82–619.

Hoekstra, H.R., Fuchs, L.H., 1956. Synthesis of coffinite–$USiO_4$. Science 123, 105.

Hoeve, J., Sibbald, T.I.I., 1978. On the genesis of Rabbit Lake and other unconformity-type uranium deposits in northern Saskatchewan, Canada. Econ. Geol. 73, 1450–1473.

Janeczek, J., Ewing, R.C., 1992. Corrosion and alteration of uraninite under reducing conditions. J. Nucl. Mater. 490, 157–173.

Janeczek, J., Ewing, R.C. 1994. Uraninite from Cigar Lake: drill cores 220 and FH-18. AECL report, 1085, pp. 93–103.

Janeczek, J., Ewing, R.C., 1995. Mechanisms of lead release from uraninite in natural fission reactors in Gabon. Geochim. Cosmochim. Acta 59, 1917–1931.

Janeczek, J., Ewing, R.C., Oversby, V.M., Werme, L.O., 1996. Uraninite and UO_2 in spent nuclear fuel: a comparison. J. Nucl. Mater. 238, 21–130.

Johnson, L.H., Werme, L.O., 1994. Materials characteristics and dissolution behavior of spent nuclear fuel. Mater. Res. Soc. Symp., 24–27.

Johnson, L.H., Shoesmith, D.W., Lunansky, G.E., Baily, M.G., Tremaine, P.R., 1982. Mechanisms of leaching and dissolution of UO_2 fuel. J. Nucl. Technol. 56, 238–253.

Kotzer, T.G., Kyser, T.K., 1993. O, U and Pb isotopic and chemical variations in uraninite: implications for determining the temporal and fluid history of ancient terrains. Am. Mineral. 78, 1262–1274.

Kotzer, T.G., Kyser, T.K., 1995. Petrogenesis of the Proterozoic Athabasca Basin, northern Saskatchewan, Canada, and its relation to diagenesis, hydrothermal uranium mineralization and paleohydrogeology. Chem. Geol. 120, 45–89.

Kotzer, T.G., Kyser, T.K., Irving, E., 1992. Paleomagnetism and the evolution of the fluids in the Proterozoic Athabasca Basin, northern Saskatchewan, Canada. Can. J. Earth Sci. 29, 1474–1491.

Langmuir, D., 1978. Uranium solution–mineral equilibria at low temperatures with application to sedimentary ore deposits. Geochim. Cosmochim. Acta 42, 547–569.

Leshin, L.A., McKeegan, K.D., Carpenter, P.K., Harvey, R.P., 1998. Oxygen isotopic constraints on the genesis of carbonates from martian meteorite ALH84001. Geochim. Cosmochim. Acta 62, 3–13.

Li, Z.X., Zhang, L., Powel, C.McA., 1996. Positions of the East Asian cratons in the Neoproterozoic supercontinent Rodinia. Aust. J. Earth Sci. 43, 593–604.

Ludwig, K.R., 1993. ISOPLOT. A plotting and regression program for radiogenic-isotope data. USGS, Open File Rep., 91–445, pp. 1–42.

Lyon, I.C., Saxton, J.M., Turner, G., 1994. Isotopic fractionation in secondary ionization mass spectrometry. Rapid Commun. Mass Spectrom. 8, 837–843.

Mallard, L.D., Rogers, J.J., 1997. Relationship of Avalonian and Cadomian terranes to Grenville and Pan-African events. J. Geodyn. 23, 197–221.

Meddaugh, W.S., 1983. Age and origin of uraninite in the Elliot Lake, Ontario uranium ores. Unpublished Ph.D. diss., Harvard University.

Reed, S.J.B., 1989. Ion microprobe analysis—a review of geological applications. Min. Mag. 53, 3–24.

Reyx, J., Ruhlmann, F., 1993. Etude metallographie des differentes associations minerales et caracterisation chimique des mineraux uraniferes du gisement de Cigar Lake (Saskatchewan, Canada). Can. J. Earth Sci. 30, 705–719.

Rogova, V.P., Belova, L.N., Kiziyarov, G.N., Kuznetsova, N.N., 1974a. Calciouranoite, a new hydroxide of uranium. Int. Geol. Rev. 16, 1255–1256.

Rogova, V.P., Belova, L.N., Kiziyarov, G.N., Kuznetsova, N.N., 1974b. Bauranoite and metacalciouranoite, new minerals of the hydrous uranium oxide group. Int. Geol. Rev. 16, 214–219.

Shimizu, N., Hart, S.R., 1982. Applications of the ion microprobe to geochemistry and cosmochemistry. Annu. Rev. Earth Planet. Sci. 10, 483–526.

Shroeer, J.M., Rhodin, T.N., Bradley, R.C., 1973. A quantum-mechanical model for the ionization and excitation of atoms during sputtering. Surf. Sci. 34, 571–580.

Sigmund, P., 1969. Theory of sputtering: I. Sputtering yield of amorphous and polycrystalline targets. Phys. Rev. 184, 383–416.

Smellie, J., Cramer, J.J., 1994. Final report of the AECL/SKB Cigar Lake analog study: AECL Report, 10851, pp. 28–50.

Smellie, J., Karlsson, F., 1996. A reappraisal of some Cigar Lake issues of importance to performance assessment. SKB Tech. Rep. (TR 96-08), Stockholm.

Smith, D.K., 1984. Uranium mineralogy. Uranium Geochemistry, Mineralogy, Geology, Exploration and Resources. The Institution of Mining and Metallurgy, London, England, pp. 43–88.

Tilton, G.R., 1960. Volume diffusion as a mechanism for discordant lead ages. J. Geophys. Res. 65, 2933–2945.

Valley, J.W., Graham, C.M., 1991. Ion microprobe analysis of oxygen isotope ratios in granulite facies magnetites: diffusive exchange as a guide to cooling history. Contrib. Miner. Petrol. 109, 38–52.

Valley, J.W., Graham, C.M., Hart, B., Eiler, J.M., Kinny, P.D., 1997. Ion microprobe analysis of oxygen, carbon, and hydrogen isotope ratios. In: McKibben, M.A., Shanks, W.C. (Eds.), Applications of Microanalytical Techniques to Understanding Mineralizing Processes. Soc. Econ. Geol. Rev., vol. 7, pp. 73–98.

Veblen, D.R., 1992. Electron microscopy applied to nonstoichiometry, polytypism, and replacement reaction minerals. In: Buseck, P.R. (Ed.), Minerals and Reactions at the Atomic Scale: Transmission Electron Microscopy. Rev. Mineral., vol. 27. Mineralogical Society of America, Chelsea, MI, pp. 181–223.

Williams, P., 1979. The sputtering process and sputtered ion emission. Surf. Sci. 90, 588–643.

Wronkiewicz, D.J., Bates, J.K., Gerding, T.J., Veleckis, E., Tani, B.S., 1992. Uranium release and secondary phase formation during unsaturated testing of UO2 at 90 °C. J. Nucl. Mater. 190, 107–127.

Yershov, V.M., 1974. A method of examining the diffusion parameters of lead in uranium minerals. Geokhimiya 10, 1565–1568.

Young, G.M., 1992. Late Proterozoic stratigraphy and the Canada–Australia connection. Geology 20, 215–218.

Yu, M.L., Lang, N., 1986. Mechanisms of atomic ion emission during sputtering. Nucl. Instrum. Methods B14, 403–413.

Zheng, Y., 1995. Isotope fractionation in uranium oxides. Nucl. Sci. Technol. 6, 193–197.

Zetterström, L., Fayek, M., Sunde, T., Schöberg, H., 2001. U and Pb isotope calibration of uraninite and galena standards for SIMS. Standards News Letter submitted for publication.